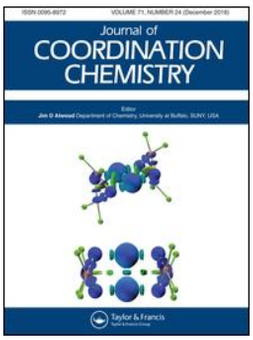

Journal of Coordination Chemistry

ISSN: (Print) (Online) Journal homepage: https://www.tandfonline.com/loi/gcoo20

Ultrasound-assisted synthesis and photophysical investigation of a heterocyclic alkylated chalcone: a sensitive and selective fluorescent chemosensor for Fe^{3+} in aqueous media

Abdullah M. Asiri , Mona Mohammad Al-Amari , Qasim Ullah & Salman A. Khan

To cite this article: Abdullah M. Asiri , Mona Mohammad Al-Amari , Qasim Ullah & Salman A. Khan (2020): Ultrasound-assisted synthesis and photophysical investigation of a heterocyclic alkylated chalcone: a sensitive and selective fluorescent chemosensor for Fe^{3+} in aqueous media, Journal of Coordination Chemistry, DOI: 10.1080/00958972.2020.1838490

To link to this article: https://doi.org/10.1080/00958972.2020.1838490

Published online: 05 Nov 2020.

JOURNAL OF COORDINATION CHEMISTRY
https://doi.org/10.1080/00958972.2020.1838490

Taylor & Francis
Taylor & Francis Group

Ultrasound-assisted synthesis and photophysical investigation of a heterocyclic alkylated chalcone: a sensitive and selective fluorescent chemosensor for Fe^{3+} in aqueous media

Abdullah M. Asiri[a,b], Mona Mohammad Al-Amari[a], Qasim Ullah[c] and Salman A. Khan[c]

[a]Chemistry Department, Faculty of Science, King Abdulaziz University, Jeddah, Saudi Arabia; [b]Center of Excellence for Advanced Materials Research (CEAMR), King Abdulaziz University, Jeddah, Saudi Arabia; [c]Physical Sciences Section, School of Sciences, Maulana Azad National Urdu University, Hyderabad, Telangana, India

ABSTRACT

Alkylated pyridine chalcone (AIPO) has been synthesized by reaction of 1-allyl-1H-indole-3-carbaldehyde with 2-acetyl pyridine. The chalcone structure was characterized by spectral and elemental analysis. The absorption and emission in ten solvents with different polarities were used to calculate the photophysical parameters for this compound. This heterocyclic fluorescent compound serves as a selective probe for recognition of Fe^{3+}. A 1:1 bonding stoichiometry between AIPO and Fe^{3+} has been detected by Benesi–Hildebrand, Stern–Volmer and Job-plot methods. The binding stoichiometric ratio was further confirmed by the density functional theory (DFT) calculations.

ARTICLE HISTORY
Received 3 March 2019
Accepted 11 September 2020

KEYWORDS
Chalcone; iron; pyridine; sensor; Stokes shift

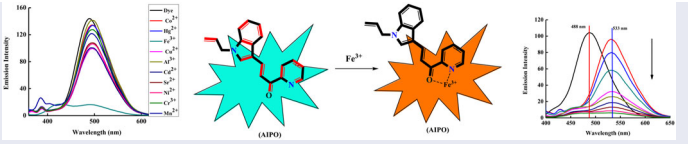

1. Introduction

Organic compounds containing electron donors and electron acceptors which can assemble into long chain conjugated frameworks are donor–acceptor chromophores with wide-ranging applications in light harvesting systems, optoelectronic devices [1], thin film solar cells [2] and photofunctional devices [3] due to their charge transfer properties within the molecule from electron donor to electron acceptor. These compounds are also used as polarity probes, laser dyes, nonlinear optics, and memory storage devices [4]. Photophysical parameters of the chromophores are important to understand the photophysical properties of molecules [5]. α,β-Unsaturated ketones,

CONTACT Salman A. Khan sahmad_phd@yahoo.co.in

known as chalcones, have been recognized for more than 100 years; the simplicity of their synthesis with their structure adaptability attracts a new attention [6]. The use of a chromophore having a ketone group in modern functional dyes has improved structure–property associations. Only recently have the photophysical properties of α,β-unsaturated ketones been studied [7]. Chalcones having carbonyl groups and donor groups such as OH, OCH_3 and N-CH_3 with the α,β-unsaturated ketones are donor π-acceptor chromophores which can give better optical properties compared to α,β-unsaturated ketones with applications in various physical sciences [8]. Chalcones having donor and acceptor groups can be used as an off–on or on–off fluorescent chemosensor for detection of toxic metals by the photo electron transfer (PET), transition charge transfer (CT), chelation-induced enhanced fluorescence (CHEF), excimer formation and fluorescence resonance energy transfer [9]. Numerous heterocyclic compounds were applied as chemosensors for recognition of metal ions. Iron has a vital role in environment, biology and chemistry, an essential trace element for human health [10, 11]. Since Fe^{3+} is a cofactor in many enzymatic reactions, it is crucial for living cells functioning in humans with other roles, including specialization in protein transport and storage [12]. The concentration of iron(III) has a major role in diseases, including diabetes, anemia, liver damage, Parkinson's disease, cancer, and hemochromatosis [13]. Therefore, there is need for an emergent molecule which can be used as a selective and sensitive fluorescent chemosensor that can differentiate Fe^{3+} when present with different transition metal ions. The detection of iron ion was achieved by many organic compounds, but synthetic hitches necessitate arduous multistep organic synthesis [14]. While there is need for selective and sensitive chemosensors in Fe^{3+} recognition, there is desire to achieve a fluorescence probe with sensing efficiency and time/cost-effectiveness. Herein, we describe the synthesis of a simple, cost effective heterocyclic chalcone with photophysical, physicochemical studies for this compound in detection of Fe^{3+}.

2. Experimental

2.1. Chemical and reagents

Starting materials such as 1H-indole-3-carbaldehyde, 1-(pyridine-2-yl) ethan-1-one, 3-bromoprop-1-ene and sodium hydroxide were obtained from Acros Organic. Additional chemicals and solvents used in this project were of analytical grade and used without purification. DMF was used to prepare the stock solution of AIPO. Metal salts used in this paper, Co^{2+}, Hg^{2+}, Fe^{3+}, Cu^{2+}, Al^{3+}, Cd^{2+}, Sr^{2+}, Ni^{2+}, Cr^{3+} and Mn^{2+}, were dissolved in double distilled water.

2.2. Instrumentation

Chalcone (AIPO) melting point was recorded by Stuart Scientific Co. Ltd. melting point apparatus. A Perkin-Elmer 100 FT-IR spectrometer was used for FT-IR spectra and a Bruker spectrometer was used to obtain ^1H and ^{13}C NMR spectra. Absorption spectra of APIO were recorded at 25 °C using a Shimadzu UV-16550PC UV/Vis spectrometer.

Fluorescence emission data were obtained from a Shimadzu RF 5301PC fluorescence spectrometer.

2.3. Synthesis of 1-allyl-1H-indole-3-carbaldehyde

At room temperature KOH pellets (1.15 g, 0.20 mol) were added to a stirred mixture of indole-3-carbaldehde (2.5 g, 0.17 mol) in 25 mL of ethanol to achieve complete dissolution. Then by vacuum filtration we eliminate ethanol from the crude product and adding 25 mL of acetone to the crude mixture, 3-bromoprop-1-ene (1.45 mL, 0.17 mol) was added to the solution. The 3-bromoprop-1-ene precipitate was achieved instantaneously. The product solid was separated by vacuum and the solution was concentrated. Crystallization from ethanol gave 1-allyl-1H-indole-3-carbaldehyde [15].

2.4. Synthesis of (E)-3-(1-allyl-1H-indol-3-yl)-1-(pyridin-2-yl) prop-2-en-1-one (AIPO)

Allyl-1H-indole-3-carbaldehyde and 1-(pyridine-2-yl) ethan-1-one were dissolved in 50 mL ethanolic solution of NaOH in a 100 mL Erlenmeyer flask. The reaction mixture was exposed to the ultrasonic generator in a water bath at 40 °C for 12 min. Completion of the reaction was monitored by TLC, then the mixture was poured into crushed ice in a 200 mL beaker and the pH adjusted to ~2 by the addition of HCl. Yellow solid was obtained, filtered by suction, washed by water, dried and crystallized in chloroform and ethanol (8:2) [16].

Brown crystals, %yield: 88.76%; m.p: 117 °C; FT-IR (cm^{-1}): ν: 3097 (C = CHstr.), 2915 (CHstr), 1655 (C = Ostr, conjugated ketone), 1572 (C = Caromatic Str), 1379 (C-Naromatic str.), 740 (1,2 disubstituted (*z*) CH = CH out of plane); ^{1}H NMR (600 MHz $CDCl_3$) δ: 8.79 (1H2, dd, J = 4.6), 7.49 (1H3, td, J = 4.7, 7.4), 8.23 (1H4, dt, J = 1.0, 7.7), 7.89 (1H5, td, J = 1.7, 7.6), 8.27 (2H8-9, d, J = 15), 7.63 (1H11, s), 8.15 (1H13, dd, J = 2.0, 5.4), 7.33–7.34 (2H14-15, m), 7.39 (1H16, dd, J = 2.0, 5.8), 4.78 (2H19, d, J = 5.4), 6.02 (1H20, m, J = 5.4, 10.8, 16.8), 5.18 (1H21, dd, J = 0.6, 17.4), 5.30 (1H21′, dd, J = 0.6, 10.2); ^{13}C NMR (600 MHz, $CDCl_3$) δ: 148.7, 121.1, 136.8, 123.1, 155.0 (pyridine moiety), 189.5 (C = O), 126.3, 138.4 (alkene moiety), 113.8, 132.2, 137.5, 126.6, 121.6, 122.7, 118.4, 116.0 (indole moiety), 49.2, 133.3, 110.3 (propene moiety); Anal. Calcd. for $C_{19}H_{16}N_2O$: C, 79.14; H, 5.59; N, 9.72. Found: C, 79.12; H, 5.55; N, 7.88.

3. Results and discussion

3.1. Chemistry

Alkylated heterocyclic chalcone (E)-3-(1-allyl-1H-indol-3-yl)-1-(pyridin-2-yl) prop-2-en-1-one (AIPO) was prepared by a two-step reaction, first alkylation of indole-3-carbaldehyde by reaction of 3-bromoprop-1-ene and then 1-allyl-1H-indole-3-carbaldehyde reacted with 2-acetyl pyridine to give AIPO (Scheme 1). The AIPO structure has been confirmed by FT-IR, ^{1}H NMR and ^{13}C NMR spectral analysis. FT-IR spectra of AIPO gave absorption bands at 1655 and 1562 cm^{-1} due to the conjugated C = O and conjugated C = C groups, respectively, which represents the characteristic peaks of AIPO.

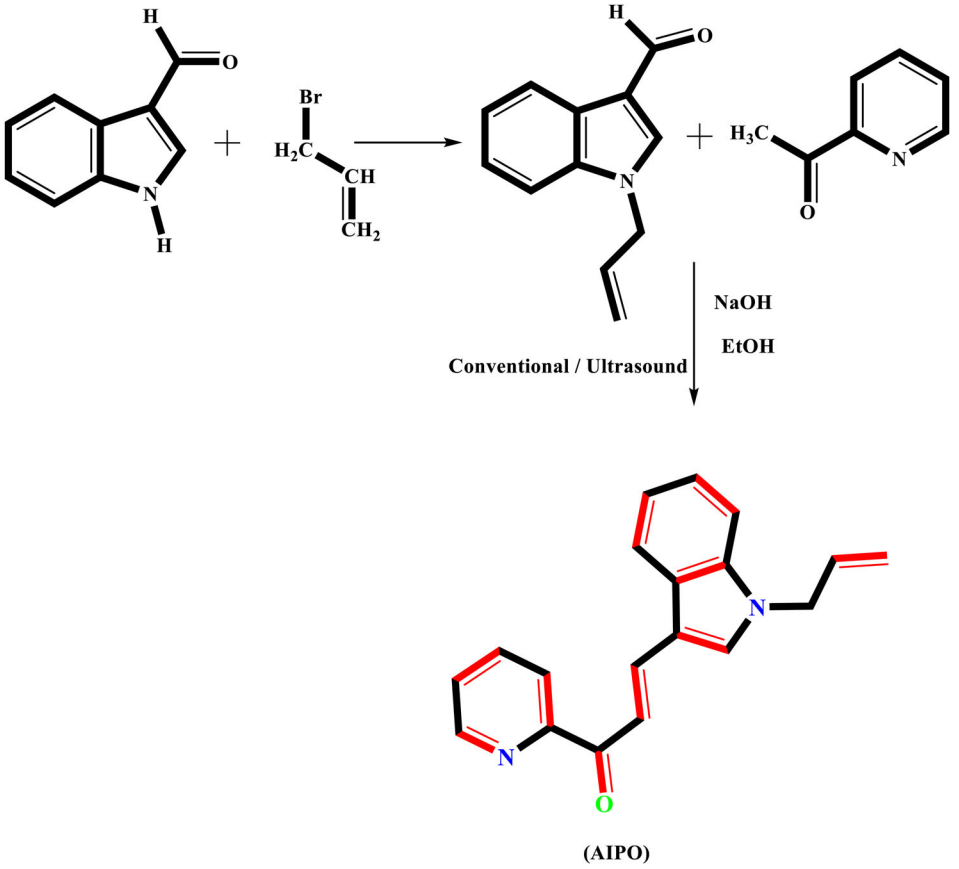

Scheme 1. Synthesis of AIPO.

Absences of a sharp peak at 3451 cm^{-1} indicates indole is converted to allyl-1H-indole. ^{1}H NMR spectra further confirmed the chalcone structure. ^{1}H NMR spectra of AIPO in $CDCl_3$ displayed characteristic peaks for α,β-unsaturated ketone in the form of a doublet at 8.27 ppm with coupling constant (*J*) 15 Hz, indicating the *trans* configuration of the alkene moiety of α,β-unsaturated ketone. Nine aromatic protons of AIPO were a singlet doublet and doublet of doublets from 7.63 to 8.79 ppm. ^{13}C NMR spectral data further confirm and identify the compound. The carbonyl carbon was at 189.5 ppm. The aromatic signals were located at 116.0–148.7 ppm and alkylated propene gave three signals at 49.2, 133.3 and 110.3 ppm for $N–CH_2–CH=CH_2$ as shown in Figure 1.

3.2. Photophysical properties of AIPO

AIPO is soluble in many solvents. Its Uv/vis spectra were recorded in ten solvents (polar to non-polar, protic, and aprotic), DMSO, DMF, ethanol, methanol, $CHCl_3$, CCl_4, CH_3CN, dioxane, THF, and *n*-hexane (Figures 2 and 3). In all the tested solvents the absorption spectra are mainly characterized by the band at 310–500 nm (Figure 2) which may be assigned $S_1 \leftarrow S_0$ (Table 1).

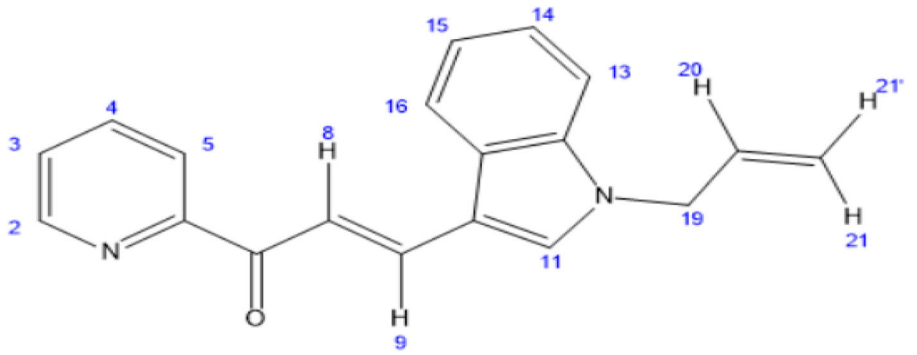

Figure 1. Structure of AIPO with numbering of hydrogen atoms.

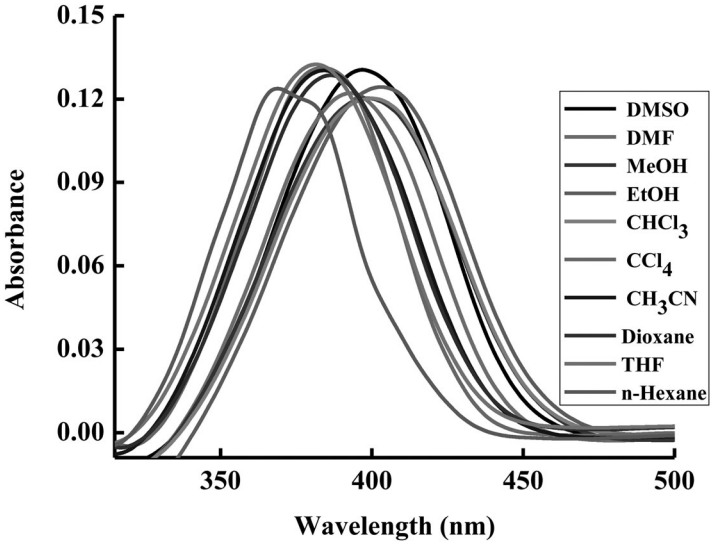

Figure 2. UV-absorbance spectra of 1×10^{-5} M of AIPO in different solvents.

The properties of solvent noticeably affected the absorption maxima of AIPO by the bathochromic shift or red shift of 25 nm when polarity of the solvents increases from *n*-hexane to DMSO, indicating the AIPO ground state has polar nature. Red shift is due to intramolecular charge transfer from donor group (1-allyl-1H-indole) to the acceptor group (pyridine ring) [17]. The AIPO emission spectra were intensely associated with solvent polarity upon excitation at 350 nm. AIPO chromophore shows one broad band (Figure 3) which indicates electronic transition $S_1 \rightarrow S_0$.

The fluorescence maxima shift to longer wavelength by increasing the solvent polarity 91 nm from *n*-hexane (402 nm) to DMSO (493 nm), implying that solvent polarity affected excited state energy of the AIPO chromophore more than the ground state, owing to a π–π^* transition [18].

The absorbance energy (E_a) and emission energy (E_f) of AIPO in various solvents correlate with the empirical Dimroth polarity parameters $E_T(30)$ of the different

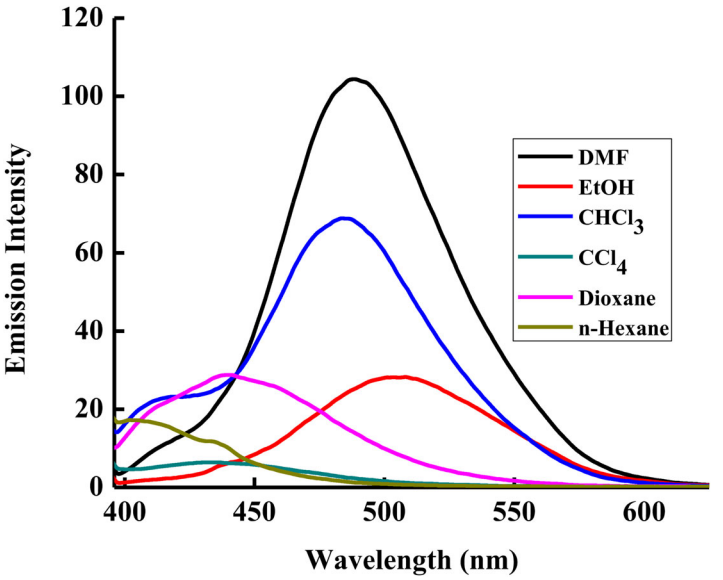

Figure 3. Fluorescence spectra of 1×10^{-5} M of AIPO in different solvents.

Table 1. Photophysical properties and fluorescence quantum yields of AIPO in various solvents.

Solvent	Δf	E_T^N	$E_T(30)$ Kcal mol^{-1}	λ_{ab} (nm)	λ_{em} (nm)	ε M^{-1} cm^{-1}	f	μ_{12} Debye	$\Delta\nu_{st}$ (cm^{-1})	Φ_f
DMSO	0.263	0.441	45.1	398	493	13,109	0. 25	4.58	4842	0.52
DMF	0.274	0.404	43.8	395	488	12,203	0.23	4.35	4825	0.50
EtOH	0.305	0.654	51.9	400	508	11,930	0.25	4.58	5315	0.13
MeOH	0.308	0.762	55.4	404	511	12,440	0.26	4.69	5183	0.099
$CHCl_3$	0.217	0.259	39.1	397	484	11,930	0.22	4.24	4527	0.33
CCl_4	0.0245	0.472	32.4	384	439	13,150	0.17	3.74	3262	0.022
CH_3CN	0.274	0.164	45.6	383	468	13,050	0.24	4.35	4742	0.45
Dioxane	0.148	0.210	36.0	386	445	12,820	0.18	3.74	3435	0.14
THF	0.209	0.006	35.1	384	438	13,100	0.17	3.60	3210	0.11
n-Hexane	0.0014	0.0002	31.1	373	402	12,150	0.10	2.81	1934	0.077

solvents as represented in Figure 4. A single dimension correlation between solvent polarity and energy of the absorption and emission was established by using the following equations [19].

$$E_a = 80.82–0.018 \times E_T(30) \quad (1)$$

$$E_f = 79.30–0.044 \times E_T(30) \quad (2)$$

3.3. Transition diploe moments and oscillator strength

From absorption and emission spectra of AIPO in different solvents we obtain the different dipole moments between singlet excited state and ground state $\Delta\mu = \mu_e - \mu_g$.

Photophysical parameters of AIPO in different solvents (Table 1) have been obtained by using the Lippert–Mataga equation [20]:

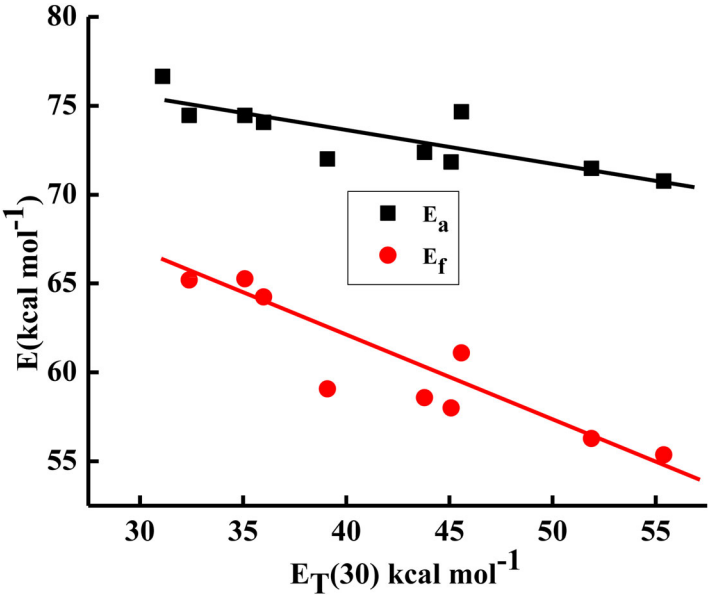

Figure 4. Plot of energy of absorption (E_a) and emission (E_f) versus $E_T(30)$ of different solvents.

$$\Delta\bar{\nu}_{st} = \nu_{abs} - \nu_{em} = \frac{2\Delta\mu^2}{hca^3}\Delta f + \text{Const.} \tag{3}$$

By increasing solvent polarity (*n*-hexane to DMSO) the Stoke shift value increases, implying that the more polar the solvent the more it stabilizes the excited state, *h* is plank's constant, the velocity of light is *c*, *a* is the radius cavity, and positioning polarizability of various solvents Δf are represented by Equation 4 [21],

$$\Delta f = \frac{\varepsilon - 1}{2\varepsilon + 1} - \frac{\eta^2 - 1}{2\eta^2 + 1} \tag{4}$$

where ε is the dielectric constant and η is refractive index of the solvents.

Figure 5 shows a linear relationship between the orientation polarizability and Stokes shift, which shows dependence of Stokes shift on the polarity of the solvent.

Lippert–Mataga was used to calculate the dipole moments ($\Delta\mu$) of AIPO (Equation 3) and a radius cavity of AIPO was calculated by Equation 5 [22],

$$a = \left(\frac{3M}{4N\pi d}\right)^{1/3} \tag{5}$$

where *M*, *N*, and *d* are molecular mass, Avogadro number, and the density of the fluorescent dye of 1 g/cm^3, respectively. Therefore, AIPO gives dipole moment of 0.81 Debye as presented in Figure 5. The positive value specified that the excited state is more polar than ground state.

Transition dipole moments of the fluorescent dye between excited state and ground state in various solvents have been calculated as Equation 6. The dipole moment values increase with increasing the solvent polarity, as shown in Table 1 [23].

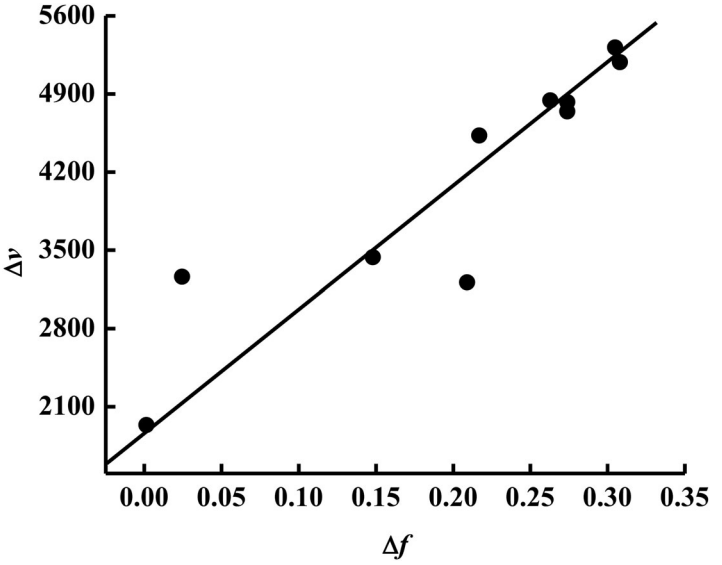

Figure 5. Plot of Δf versus Stokes shift.

$$\mu^2 = \frac{f}{4.72 \times 10^{-7} E_{max}} \tag{6}$$

E_{max} is the maximum energy of the absorption in cm^{-1}, f is the oscillator strength, and μ is the transition dipole moment.

Equation 7 has been used to calculate the oscillator strength f of the fluorescent dye AIPO in various solvents,

$$f = 4.32 \times 10^{-9} \int \varepsilon(\bar{\nu}) d\bar{\nu} \tag{7}$$

where $\bar{\nu}$ and ε are the wavenumber and the dielectric constant (M^{-1} cm^{-1}). The oscillator strength value of AIPO calculated in different solvents is listed in Table 1, and value of oscillator strength of AIPO increases by increasing solvent polarity from *n*-hexane to DMSO.

3.4. Fluorescence quantum yields of AIPO

The standard dye quinine sulfate ($\phi_r = 0.55$ in 0.1 M H_2SO_4 solution) was used as reference to calculate the fluorescence quantum yields of the heterocyclic chalcone (AIPO) in various solvents by using Equation 8 [24],

$$\Phi_f = \Phi_r \frac{I \times A_r \times n^2}{I_r \times A \times n_r^2} \tag{8}$$

where ϕ_r is the fluorescence quantum yield of quinine sulfate and ϕ_f is the AIPO calculated fluorescence quantum yield in the solvents. The absorbance of AIPO and reference dye at the excited wavelength are represented by A, I is the integrated emission intensity and n is the solvent refractive index (Table 1). The calculated value of AIPO

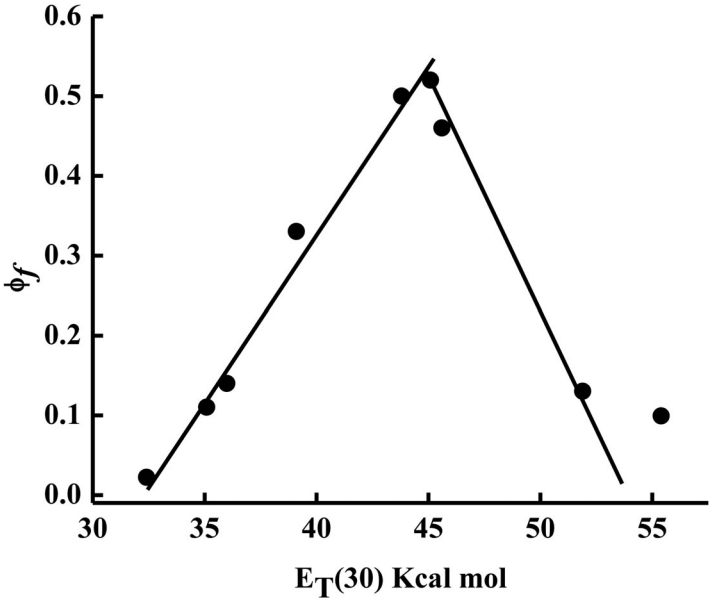

Figure 6. Plot of ϕ_f versus $E_T(30)$ of AIPO in different solvents.

fluorescence quantum yield demonstrates that the value depends on solvent polarities since the emission spectra were affected by solvent polarity. Figure 6 demonstrates the correlation between AIPO fluorescence quantum yield in various solvents and $E_T(30)$ of those solvents [25]; the solvent polarity parameter represented by $E_T(30)$ was identified by Reichardt. The data show increasing solvent polarity increased in ϕ_f due to negative solvatokinetic effects. Another factor affecting the ϕ_f values is hydrogen bonding between the allyl of AIPO and the solvent. This hydrogen bond is responsible for the decrease of ϕ_f in polar protic solvents like MeOH due to radiation-less processes. This positive solvatokinetic effect from the DMSO to polar protic solvents is from strong ICT interaction between solvent and excited chromophore [26].

3.5. Selective fluorescent chemosensor of AIPO for metal ion

The AIPO chromophore has been applied as a fluorescent chemosensor for metal ion recognition. AIPO was examined for its selectivity toward ten metal ions by emission spectra. Stock solution (1×10^{-5} M) in DMF/water (9:1) (v/v) of Co^{2+}, Hg^{2+}, Fe^{3+}, Cu^{2+}, Al^{3+}, Cd^{2+}, Sr^{2+}, Ni^{2+}, Cr^{3+} and Mn^{2+} were prepared. When excited at 385 nm, the emission spectra of AIPO exhibited exceptionally strong peak and the intensity was maintained even after addition of nine equiv. of Co^{2+}, Hg^{2+}, Cu^{2+}, Al^{3+}, Cd^{2+}, Sr^{2+}, Ni^{2+}, Cr^{3+} and Mn^{2+} (Figure 7). However, the fluorescence intensity of AIPO decreased eight-fold after addition of the same amount of Fe^{3+}, an observed quenching in emission intensity up to 80% with clear color change from yellow to dark brown (Figure 8). AIPO (ϕ_f) in absence and presence of Fe^{3+} is 0.52 and 0.099, respectively; the yield is low after adding Fe^{3+}. This quenching in fluorescent intensity of AIPO following the addition of Fe^{3+} is due to complex formation between AIPO and Fe^{3+}. AIPO photophysical properties show sensitivity toward interacting molecule due to AIPO having

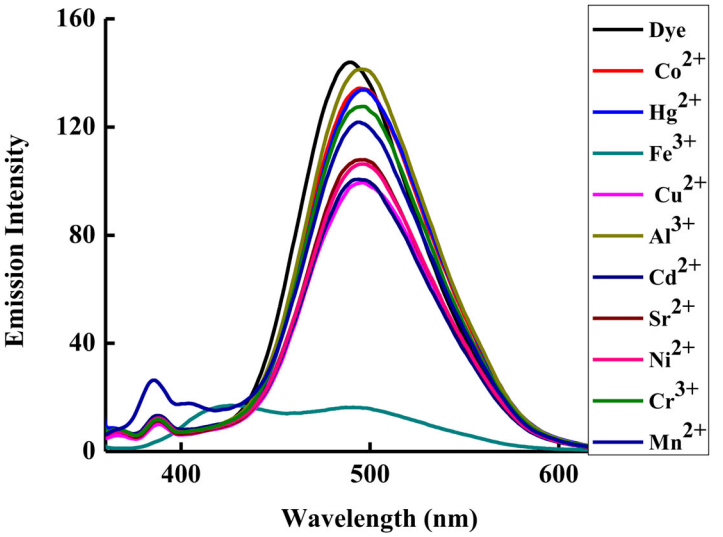

Figure 7. Emission spectra of 1×10^{-5} M of AIPO upon addition of 5.0×10^{-5} M of Co^{2+}, Hg^{2+}, Fe^{3+}, Cu^{2+}, Al^{3+}, Cd^{2+}, Sr^{2+}, Ni^{2+}, Cr^{3+}, and Mn^{2+}.

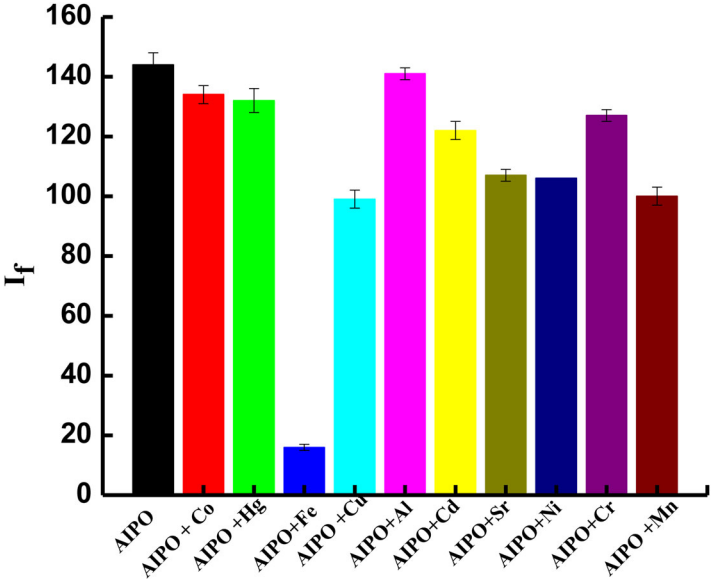

Figure 8. Emission of AIPO in the presence of different metal ion.

charge transfer (CT) structure. The nitrogen of the pyridine and the oxygen of carbonyl are the binding site between AIPO and Fe^{3+} which induce the ICT from the electron donor's nitrile and oxygen to Fe^{3+}. This complexation led to the ligand to metal charge transfer (LMCT), accountable for the quenching in fluorescence intensity (Scheme 2). Failure of the other nine metal ions to achieve this complexation with the chalcone can be explained by unsuitable ion radius [27].

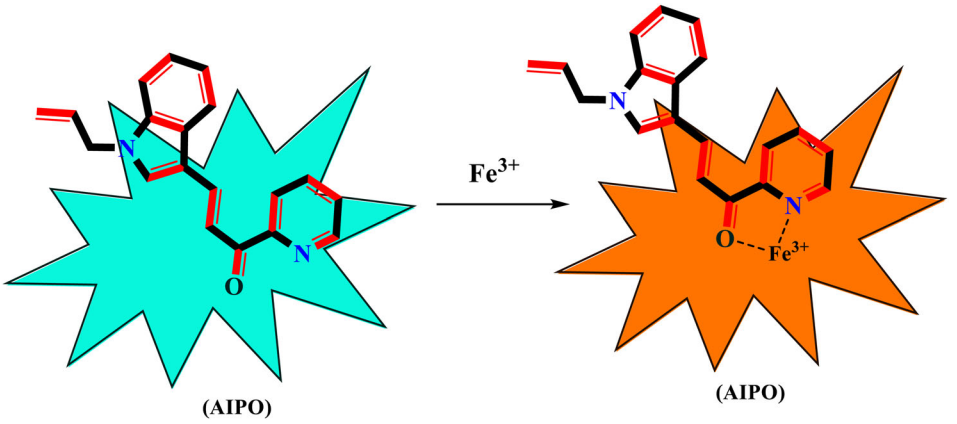

Scheme 2. Fluorescent chemosensor behavior of AIPO with Fe^{3+}.

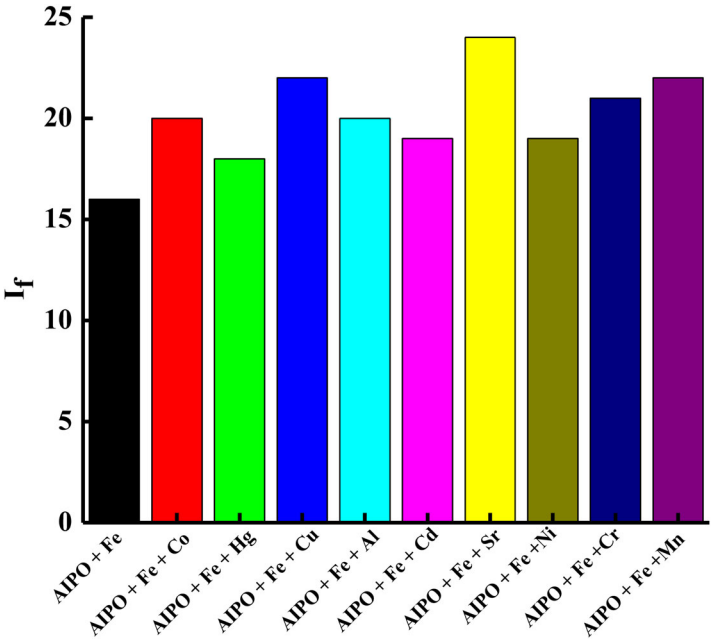

Figure 9. Competitive experiments in the AIPO + Fe^{3+} system with interfering metal ion.

Testing the selectivity of an indicator is important for the practical applicability of sensors and can be examined by the anti-Jamming ability. The possibility of interference of Co^{2+}, Hg^{2+}, Cu^{2+}, Al^{3+}, Cd^{2+}, Sr^{2+}, Ni^{2+}, Cr^{3+} and Mn^{2+} ions with Fe^{3+} ion was tested through a competition experiment. Figure 9 shows the result when examining the intensity change of AIPO (1×10^{-5} M) at 385 nm when adding 5×10^{-5} M of Fe^{3+} and (1×10^{-5} M) of the other ions. The results imply that AIPO has highly sensing selectivity toward Fe^{3+} because the competitive metal ion present did not interfere with sensing the Fe^{3+}. Thus, the heterocyclic chalcone (AIPO) is a fluorescent chemosensor for Fe^{3+} with high selectivity.

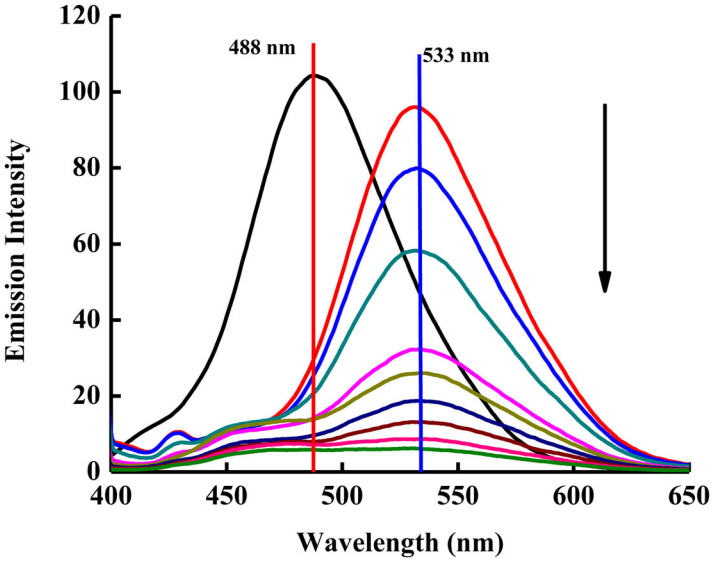

Figure 10. Emission spectra of AIPO (1×10^{-5} M) exposed to various concentrations of Fe^{3+} in DMF:water (9:1) v/v.

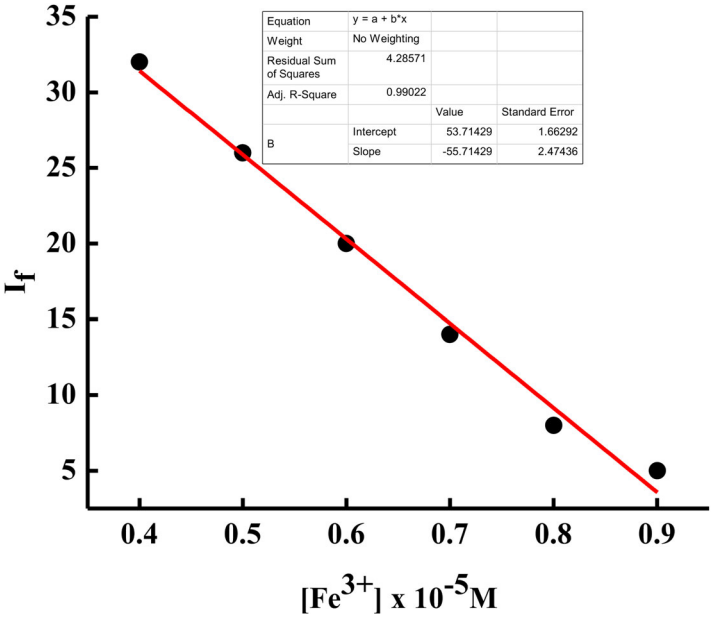

Figure 11. Fluorescence titration curve of AIPO (1×10^{-5} M) with Fe^{3+} in aqueous solution.

By gradual titration, the fluorescence quenching behavior of AIPO with Fe^{3+} shows decreased intensity by increasing Fe^{3+} concentration, and when Fe^{3+} is about 9×10^{-5} M the fluorescence intensity of AIPO reached the minimum values, owing to AIPO complexation with Fe^{3+} (Figure 10). Figure 11 illustrates that by decreasing the Fe^{3+} concentration to 4 to 9×10^{-5} M the emission intensity of the probe AIPO was

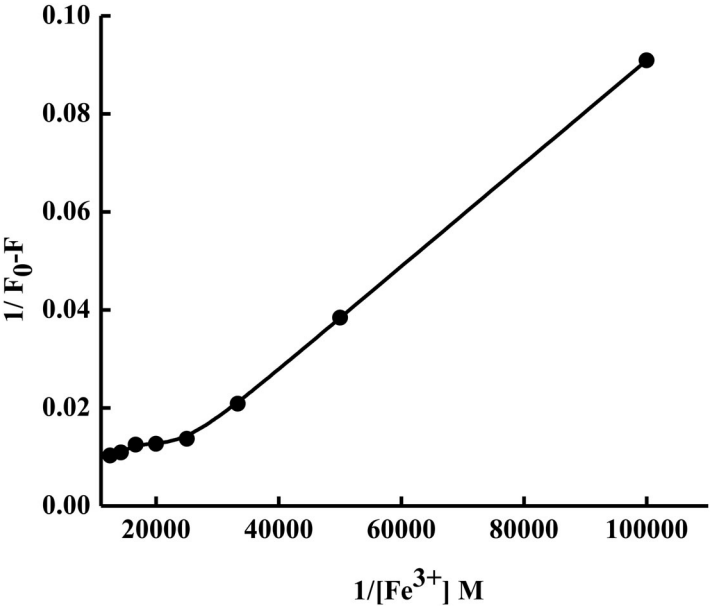

Figure 12. Benesi–Hildebrand plot for AIPO (1×10^{-5} M) at various concentrations of Fe^{3+}.

quickly reduced; the good linear response ($R = 0.99$) allows quantitative evaluation of coordination between the probe and Fe^{3+}.

Equation 9 represents the Benesi–Hildebrand plot of the binding stoichiometry and the association constant K between the chemosensor and Fe^{3+} [28].

$$\frac{1}{F^o - F'} = \frac{1}{F^o - F'} + \frac{1}{K_{app}} \times \frac{1}{(F^o - F')[Fe^{3+}]} \tag{9}$$

K_{app} is the association constant, F and F_o are the intensity of fluorescence for AIPO in the absence and presence of Fe^{3+}, respectively. When plotting $1/(F_o - F)$ vs. $1/Fe^{3+}$ the linearity proved that the complexation between metal–ligand is 1:1 stoichiometric ratio as given in Figure 12. The 1:1 binding stoichiometric of metal–ligand was strongly supported by linear fitting of the experiment plot with a coefficient over 0.98; the fitted curve is almost superimposed over the experimental plot. The estimated value of the binding constant between metal–ligand is 8.92×10^{-6} M^{-1}.

The Stern–Volmer relationship was used to help understand the fluorescence quenching behavior of AIPO sensor with Fe^{3+}; the Stern–Volmer analysis of intensity quenching of the sensor is given by Equation 10 [29],

$$\frac{I_o}{I} = 1 + K_{sv}[Fe^{3+}] \tag{10}$$

where I_o is the intensity of the fluorescence from AIPO without the presence of Fe^{3+} ion and I is the intensity of the fluorescence from AIPO when Fe^{3+} is present, and K_{sv} is Stern–Volmer constant. Figure 13 shows the Stern–Volmer plot with K_{sv} of $5.13 \times 10^{-4}\,M^{-1}$, R^2 equal 0.98. The Stern–Volmer constant value indicates that the interaction between AIPO and Fe^{3+} is efficient.

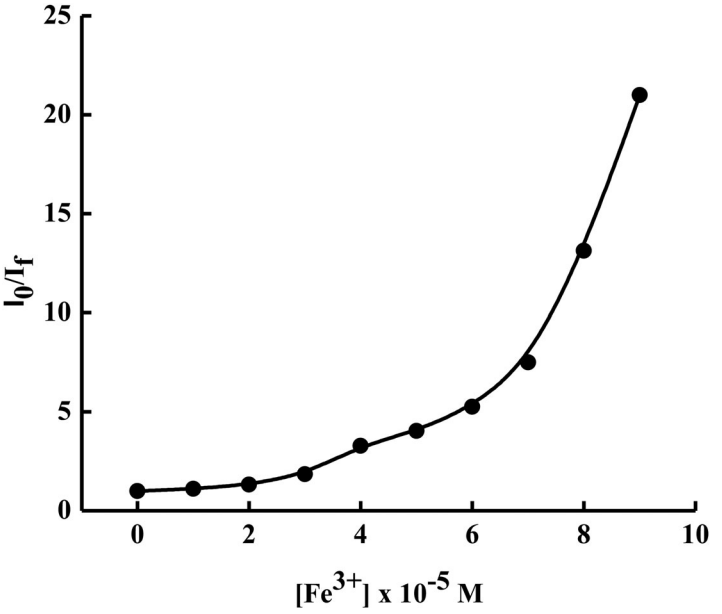

Figure 13. Stern–Volmer plot for AIPO (1×10^{-5} M) at different concentrations of Fe^{3+}.

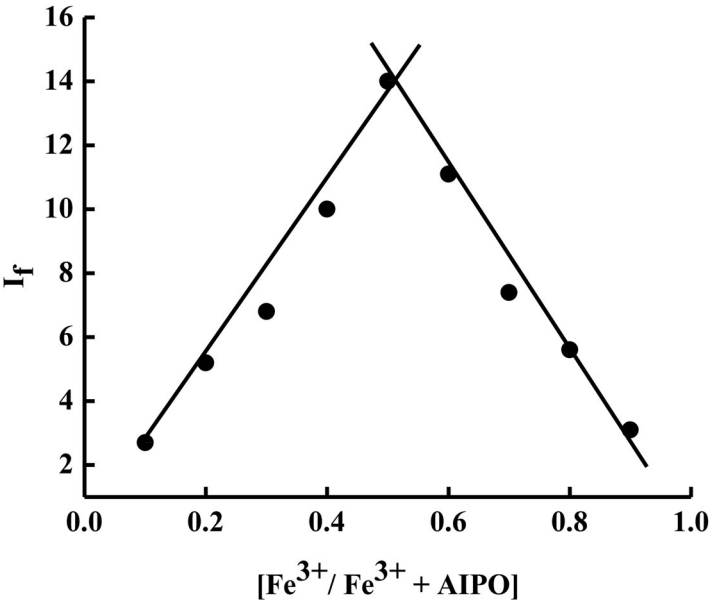

Figure 14. Job's plot of fluorescence intensity versus mole fraction of Fe^{3+}.

The stoichiometry of AIPO and Fe^{3+} was estimated by Job's plot [30]. The Job's plot was drawn by plotting mole fraction of Fe^{3+} versus fluorescence intensity as presented in Figure 14. When the mole fraction of Fe^{3+} was 0.5 the plot began to decrease, indicating that complex stoichiometry of Fe^{3+} and AIPO is 1:1. This behavior was further supported by density functional theory (DFT) calculations using 09 program on AIPO and the iron 1:1 complex; their corresponding energies are

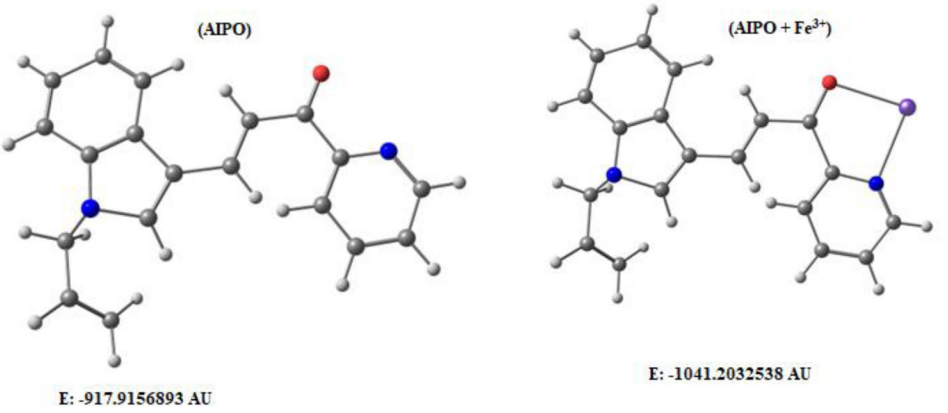

Figure 15. Conformation of AIPO (left) and AIPO·Fe^{3+} (right) optimized by density functional theory calculations.

−917.9156893 AU and −1041.2032538 AU, respectively, as shown in Figure 15, suggesting that the 1:1 stoichiometry is stable.

4. Conclusion

The reaction of 1-allyl-1H-indole-3-carbaldehyde with 2-acetyl pyridine produced the heterocyclic chalcone (E)-3-(1-allyl-1H-indol-3-yl)-1-(pyridin-2-yl) prop-2-en-1-one (AIPO). The oscillator strength, diploe moment, Stokes shift, and fluorescence quantum yields have been calculated in ten solvents on the basis of the polarity of the solvent by the absorption and emission, giving information about the interaction between the chromophore with different polarity of solvents. The heterocyclic chalcone is a turn-off fluorescent chemosensor for Fe^{3+}, with much higher selectivity over competitive metal ions. The Benesi–Hildebrand, Stern–Volmer and Job's plots have been used to explain the complexation between AIPO and Fe^{3+} in 1:1 ratio. Binding stoichiometric ratio was further conformed by the density functional theory (DFT) calculations.

Disclosure statement

No potential conflict of interest was reported by the authors.

Funding

This project was funded by the Deanship of Scientific Research (DSR) at King Abdulaziz University, Jeddah, Saudi Arabia under grant no. KEP-PhD-19-130-41. The authors, therefore, acknowledge with thanks DSR for technical and financial support.

References

[1] M. Taghi Sharbati, M.N. Soltani Rad, S. Behrouz, A. Gharavi, F. Emami. *J. Lumin.*, **131**, 553 (2011).
[2] Z. Yao, M. Zhang, H. Wu, L. Yang, R. Li, P. Wang. *J. Am. Chem. Soc.*, **137**, 3799 (2015).

[3] L. Wang, J.T. Ye, H.Q. Wang, H.M. Xie, Y.Q. Qiu. *J. Phys. Chem. C*, **121**, 21616 (2017).
[4] P.M. DiCarmine, T.B. Schon, T.M. McCormick, P.P. Klein, D.S. Seferos. *J. Phys. Chem. C*, **118**, 8295 (2014).
[5] M. Jai, X. Ma, L. Yan, H. Wang, Q. Guo, X. Wang, Y. Wang, X. Zhan, A. Xia. *J. Phys. Chem. A*, **15**, 7345 (2010).
[6] K. Yahata, M. Minami, K. Watanabe, H. Fujioka. *Org. Lett.*, **16**, 3680 (2014).
[7] A.M. Asiri, S.A. Khan, H.M. Basisi. *J. Taiwan Inst. Chem. E*, **59**, 457 (2016).
[8] K. Rurack, J.L. Bricks, G. Reck, R. Radeglia, U.R. Genger. *J. Phys. Chem. A*, **104**, 3087 (2000).
[9] K. Velmurugan, J. Prabhu, L. Tang, T. Chidambaram, M. Noel, S. Radhakrishnan, R. Nandhakumar. *Anal. Methods*, **6**, 2883 (2014).
[10] P.T. Bhattacharya, S.R. Misra, M. Hussain. *Scientifica (Cairo)*, **2016**, 5464373 (2016).
[11] J.J.R. Frausto da Silva, R.J.P. Williams. *The Biological Chemistry of the Elements: The Inorganic Chemistry of Life*, Oxford University Press, New York, Vol. 344 (1991).
[12] Y. Wang, H.Q. Chang, W.N. Wu, X.L. Zhao, Y. Yang, Z.Q. Xu, Z.H. Xu, L. Jia. *Sens. Actuat. B*, **239**, 60 (2017).
[13] M.J. Kotze, D.P. Velden, S.J. Rensburg, R. Erasmus. *EJIFCC*, **20**, 108 (2009).
[14] S.A. Khan. *J. Mol. Struct.*, **1211**, 128084 (2020).
[15] A.M. Asiri, S.A. Khan, H.M. Basisi. *Int. J. Electrochem. Sci.*, **10**, 6092 (2015).
[16] A.M. Asiri, H.M. Marwani, K.A. Alamry, M.S. Al-Amoudi, S.A. Khan, S.A. El-Daly. *Int. J. Electrochem. Sci.*, **9**, 799 (2014).
[17] R. Nandy, S. Sankararaman. *Beilstein J. Org. Chem.*, **6**, 992 (2010).
[18] U. Subuddhi, S. Haldar, S. Sankararaman, A.K. Mishra. *Photochem. Photobiol. Sci.*, **5**, 459 (2006).
[19] C. Reichardt. *Chem. Rev.*, **94**, 2319 (1994).
[20] S.M. Song, D. Ju, J.F. Li, D.X. Li, Y.L. Wei, C. Dong, P. Lin, S. Shuang. *Talanta*, **77**, 1707 (2009).
[21] N. Mataga. *BCSJ*, **36**, 654 (1963).
[22] C. Katan, S. Tretiak, M.H.V. Werts, A.J. Bain, R.J. Marsh, N. Leonczek, N. Nicolaou, E. Badaeva, O. Mongin, M. Blanchard-Desce. *J. Phys. Chem. B*, **111**, 9468 (2007).
[23] S.A. Khan, A.M. Asiri, N.S.M. Al-Ghamdi, M.E.M. Zayed, K. Sharma, H. Parveen. *J. Mol. Struct.*, **1139**, 137 (2017).
[24] A. Al Sabahi, S.N. Al Busafi, F.O. Suliman, S.M. Al Kindy. *J. Mol. Liq.*, **307**, 112967 (2020).
[25] K. Rurack, M.L. Dekhtyar, J.L. Bricks, U. Resch-Genger, W. Rettig. *J. Phys. Chem. A*, **103**, 9626 (1999).
[26] Z. Xu, G. Bai, C. Dong. Spectrochim. *Acta*, **62**, 9987 (2005).
[27] J.S. Wu, W.M. Liu, X.Q. Zhuang, F. Wang, P.F. Wang, S.L. Tao, X.H. Zhang, S.K. Wu, S.T. Lee. *Org. Lett.*, **9**, 33 (2007). (2006
[28] P.K. Chung, S.R. Liu, H.F. Wang, S.P. Wu. *J. Fluoresc.*, **23**, 1139 (2013).
[29] G.T. Selvan, C. Varadaraju, R.T. Selvan, I.V.M.V. Enoch, P.M. Selvakumar. *ACS Omega*, **3**, 7985 (2018).
[30] K.M. Vengaian, C.D. Britto, K. Sekar, G. Sivaraman, S. Singaravadive. *Sens. Actuat. B Chem.*, **235**, 232 (2016).